An Exact Lagrangian-Mean Wave Activity for Finite-Amplitude Disturbances to Barotropic Flow on the Sphere

ABRAHAM SOLOMON[1] †,
AND N. NAKAMURA[1]

[1]Department of the Geophysical Sciences, University of Chicago, 5734 S. Ellis Ave., Chicago, IL 60637, USA

(Received ?? and in revised form ??)

The finite-amplitude Rossby wave activity introduced recently by Nakamura et al. measures disturbances in terms of the areal displacement of potential vorticity (PV) from zonal symmetry and possesses exact Eliassen-Palm and nonacceleration theorems. This article investigates both theoretically and numerically how this wave activity, denoted A^*, relates to previously defined quantities such as the generalized Lagrangian mean (GLM) pseudomomentum density and the impulse-Casimir (IC) wave activity in the context of barotropic flow on the sphere. It is shown that under the barotropic constraint both the new and GLM formalisms derive the nonacceleration theorem from the conservation of Kelvin's circulation, but the two differ in the way the circulation is partitioned into a mean flow and wave activity/pseudomomentum density. The new wave activity differs from the (negative of) GLM pseudomomentum density by the Stokes correction to angular momentum density, which is not negligible even at small amplitude limit. In contrast, A^* converges to the IC wave activity and the familiar linear pseudomomentum density in the conservative small-amplitude limit, provided that their reference states are identical. Both the GLM pseudomomentum density and the zonal-mean IC wave activity may be cast into a flux conservation form in equivalent latitude, which may then be related to an exact Eliassen-Palm theorem through a gauge transformation. However, of the three wave activity forms, only A^* satisfies an exact nonacceleration theorem for the zonal-mean zonal wind $\bar{u}$. A simple jet forcing experiment is used to examine the quantitative differences among these diagnostics. In this experiment, A^* and the IC wave activity behave similarly in the domain average; however, they differ substantially in the local profiles, the former being more closely related to the flow modification. Despite their close conceptual relationship, the GLM pseudomomentum fails to capture the meridional structure of A^* because the Stokes correction term dominates the former. This demonstrates various advantages of A^* as a diagnostic of eddy-mean flow interaction.

Key Words: wave activity, potential vorticity, Kelvin's circulation, Lagrangian-mean, barotropic

---

1. Introduction

The bulk of fluid dynamics, both theory and modeling, has been developed in an Eulerian framework. Since the pioneering work of Reynolds (1895), eddies have typically

† Present Address: The University of Chicago, 5734 S. Ellis Ave. Chicago, IL 60637,USA.

been defined as the departure from some spatial or temporal average. If we define the Eulerian zonal mean of a scalar field $\chi(\lambda, \mu, t)$ on the surface of a sphere as

$$\overline{\chi}(\mu, t) = \frac{1}{2\pi} \int_0^{2\pi} \chi(\lambda, \mu, t) \mathrm{d}\lambda, \tag{1.1}$$

where λ is longitude, $\mu = \sin\phi$, $\phi \in [-\pi/2, \pi/2]$ is latitude, and t is time, then the eddy component is given by

$$\chi'(\lambda, \mu, t) = \chi(\lambda, \mu, t) - \overline{\chi}(\mu, t). \tag{1.2}$$

This decomposition forms a basis for our understanding of wave properties and the interactions of eddies with mean flows in geophysical fluids. In particular, the conservation of *pseudomomentum* is fundamental to our understanding of atmospheric circulation (e.g. Vallis 2006 §§7,12). The local conservation of pseudomomentum density A may be written as

$$\frac{\partial A}{\partial t} + \nabla \cdot \mathbf{F} = 0, \tag{1.3}$$

where $\mathbf{F}$ is a flux. Terms may be added to the right-hand side of this exact conservation relation to account for nonconservative processes in the relevant equation of motion as we will see in §4 or errors of approximation discussed below.

Linear pseudomomentum density can be defined in terms of small wavy departures of vorticity ω from a time-independent, zonally uniform reference state ω_R, $\zeta' \equiv \omega - \omega_R$. (Here $\omega_R = \overline{\omega}$ but we use the subscript R to emphasize the time independence.) For example, for barotropic flow on a sphere of radius a (Held & Phillips 1987)

$$A_L(\mu, t) = \frac{a}{2\cos\phi} \frac{\overline{\zeta'^2}}{d\omega_R/d\mu}. \tag{1.4}$$

The quantity A_L is the negative of pseudomomentum density but we will call it simply *wave activity*, following the standard nomenclature. In the absence of friction and other nonconservative effects A_L satisfies the generalized Eliassen-Palm (E-P) theorem (Andrews *et al.* 1987)

$$\frac{\partial A_L}{\partial t} + \overline{v'\zeta'} = O(\alpha^3), \tag{1.5}$$

where v is the meridional component of the flow velocity and α is a measure of eddy amplitude. The right-hand side includes the advection of A_L by the eddies. Wave activity is related to the zonal-mean zonal velocity $\overline{u}$ through the second term, the poleward flux of vorticity by the eddies:

$$\frac{\partial \bar{u}}{\partial t} = \overline{v'\zeta'} = -\frac{\partial A_L}{\partial t} + O(\alpha^3) \quad \Rightarrow \quad \frac{\partial}{\partial t}(\bar{u} + A_L) = O(\alpha^3). \tag{1.6}$$

Thus, in the conservative, small-amplitude limit the zonal-mean flow remains unchanged if wave activity is steady, a result accurate through $O(\alpha^2)$. This is the simplest form of the nonacceleration theorem due to Charney & Drazin (1961). In a balanced flow the eddy vorticity flux may be expressed as the convergence of eddy momentum flux (or equivalently, the divergence of the Eliassen-Palm (E-P) flux) through Taylor's identity

$$\overline{v'\zeta'} = -(a\cos\phi)^{-1} \frac{\partial}{\partial \mu} \{\overline{u'v'}(1-\mu^2)\}. \tag{1.7}$$

With this identity (1.5) may be recast in the form of (1.3). The vorticity flux $\overline{v'\zeta'}\cos\phi$ vanishes upon integration over the domain, which, together with (1.6), leads to the con-

servation of the domain-integrated $A_L \cos\phi$ (accurate through $O(\alpha^2)$) and $\overline{u}\cos\phi$ (exact). The global conservation of $A_L \cos\phi$ is a key to formulating certain linear stability theorems (Kuo 1949; Rayleigh 1896; Vallis 2006 §7).

An effort to extend (1.5) to a finite-amplitude regime while maintaining the Eulerian description of the flow is due to Killworth & McIntyre (1985), McIntyre & Shepherd (1987), and Haynes (1988). These authors construct a finite-amplitude wave activity that obeys an exact local flux conservation (1.3) by combining Kelvin's impulse and Casimir functions associated with absolute vorticity (or potential vorticity, PV). The *impulse-Casimir (IC) wave activity* is measured relative to an arbitrary, zonally symmetric reference state that does not depend on time. The IC wave activity is $O(\alpha^2)$ as $\alpha \to 0$ and its zonal average converges to the linear wave activity (1.4) in this limit, provided that the same reference state is used. The global conservation of IC wave activity allows one to derive finite-amplitude stability theorems for shear flows (McIntyre & Shepherd 1987; Shepherd 1988, 1989). However, the $O(\alpha^3)$ term in (1.6) becomes locally dominant at large amplitudes, undermining the role of IC wave activity as a driver of the mean flow. Also, the definition of IC wave activity depends on the choice of the reference state, which is not *a priori* obvious for the real atmosphere. For these reasons, application of the IC wave activity was initially limited to model simulations, where the diagnostic provided insights into the evolution of instabilities, wave breaking and the reflection of Rossby wave trains (Scinocca & Peltier 1994; Brunet & Haynes 1996; Magnusdottir & Haynes 1996, 1999). More recently, Strong & Magnusdottir (2008) applied the IC wave activity to observed atmospheric flows. Although their analysis was performed for a composite of many events, Strong and Magnusdottir were able to demonstrate the usefulness of finite-amplitude wave activity for understanding a complex wave breaking phenomenon.

A significant conceptual advantage may be gained if one switches to a Lagrangian perspective. The generalized Lagrangian mean (GLM) theory (Andrews & McIntyre 1978*a*,*c*; McIntyre 1980) defines a mean state by averaging quantities over selected material volumes. For example, Lagrangian-mean properties of a wavy material tube displaced from a zonal circle may be described as a function of its center-of-mass latitude, ϕ_m. In particular, the relationship between the GLM angular momentum and pseudomomentum densities at ϕ_m is analogous to (1.6) yet *exact*, that is, there is no residual on the right-hand side (Andrews & McIntyre 1978*a*; see also (2.16) below). This allows one to interpret pseudomomentum density as the driver of the mean flow even at finite amplitude. However, at finite amplitude the center-of-mass latitude may not be mapped to geometrical latitude one-to-one (see figure 6b below) and thus becomes unsuitable as a meridional coordinate. To circumvent this problem, McIntyre (1980) suggested the use of the PV contours as a quasi-material meridional coordinate (*modified Lagrangian mean*). While PV is generally a monotonic function of latitude, it may not sample the globe uniformly as its gradient becomes inhomogenous in the presence of a flow and nonconservative processes (see figure 6a). For this reason, it is deemed more practical to adopt *equivalent latitude*, a measure of mass (area) enclosed by the PV contours on an isentropic surface, scaled to the real latitude (McIntyre 1982; Butchart & Remsberg 1986). Although the equivalent latitude gained popularity in the analysis of stratospheric transport (Allen & Nakamura 2003), to the authors's knowledge, the GLM theory has never been reformulated for equivalent latitude. For a baroclinic atmosphere, some flavor of the GLM theory is retained in the *transformed Eulerian mean* (TEM) formalism of Andrews & McIntyre (1976, 1978*b*), in which the Lagrangian-mean motion in the meridional plane is characterized by the *residual circulation*. The TEM formalism – the generalized E-P flux and its divergence in particular – has been widely used to diagnose wave-mean flow

interaction (e.g., Edmon *et al.* 1980). See Bühler (2009) for a comprehensive review of the GLM theory.

Recently, Nakamura & Zhu (2010*a*,*b*) (hereafter referred to as NZ10ab) and Nakamura & Solomon (2010, 2011) (NS10 and NS11 hereafter) introduced a finite-amplitude wave activity based on the instantaneous areal displacement of PV contours from zonal symmetry. In the context of barotropic flow on the sphere,

$$A^*(\mu_e,t) = \frac{1}{2\pi a\cos\phi_e}\left(\iint\limits_{\omega\geqslant\omega_e}\omega dS - \iint\limits_{\mu\geqslant\mu_e}\omega dS\right), \tag{1.8}$$

where $dS = a^2 d\lambda d\mu$ is the area element, $\omega = 2\Omega\mu + \zeta$ is the absolute vorticity (Ω is the rotation rate of the sphere and ζ is relative vorticity), and ω_e is the value corresponding to equivalent latitude μ_e, i.e., the latitude of the ω-contour in an eddy-free reference state after ω is 'zonalized' without changing the enclosed area. Measuring the departures from a mean state which is independent of longitude, this finite-amplitude wave activity is the negative pseudomomentum density defined in equivalent latitude coordinate. With the Stokes theorem the two integrals in (1.8) can be expressed as Kelvin's circulation about the material vorticity contour $C(\omega(\mu_e,t))$ and the circulation around the circle of equivalent latitude $C(\mu_e,t)$

$$A^*(\mu_e,t) = \frac{1}{2\pi a\cos\phi_e}(C(\omega(\mu_e,t)) - C(\mu_e,t)). \tag{1.9}$$

It is easy to show (NZ10a, NS10) that $A^* \geqslant 0$ for an arbitrary geometry of the ω-contour and (e.g., appendix of NS10) that the small-amplitude, conservative limit of A^* equals A_L if ω_R in (1.4) is taken as the absolute vorticity as a function of μ_e, which is invariant with time. Furthermore, in the conservative (but finite-amplitude) limit, A^* satisfies *exact* Eiassen-Palm (E-P) and nonacceleration theorems

$$\frac{\partial A^*}{\partial t} + \overline{v'\zeta'} = 0, \qquad \frac{\partial}{\partial t}(\bar{u} + A^*) = 0 \tag{1.10}$$

at each μ_e. The latter result arises naturally if one applies Kelvin's theorem to (1.9) and notes that $(2\pi a\cos\phi_e)^{-1}C(\mu_e,t) = \bar{u}(\mu_e,t) + \Omega a\cos\phi_e$.

By integrating (1.10) with time from a hypothetical eddy-free reference state $(\bar{u}, A^*) = (u_{ref}, 0)$ to the current observed state $(\bar{u}_{obs},\ A^*_{obs})$, one can quantify the adjustment to the mean flow, or the departure from the reference state, in terms of the observed wave activity

$$\Delta u \equiv \bar{u}_{obs} - u_{ref} = -A^*_{obs}, \tag{1.11}$$

which can be evaluated with instantaneous data using (1.8). The above formalism has been extended to a baroclinic atmosphere and applied to reanalysis data to quantify the quasi-adiabatic adjustment in the general circulation of the atmosphere due to finite-amplitude eddies (NS10, NS11). Furthermore, (1.10) implies that the reference state flow

$$u_{ref}(\mu_e) \equiv \overline{u} + A^* = \frac{1}{2\pi a\cos(\phi_e)}\left(\iint\limits_{\omega\geqslant\omega_e}\omega dS - \iint\limits_{\mu\geqslant\mu_e} 2\Omega\mu dS\right) \tag{1.12}$$

is time-independent in the conservative limit, and more generally, it responds only to forcing and dissipation and filters out the exchange between $\overline{u}$ and A^* through the E-P flux divergence. Similar to previous diagnostics of circulation based on the distribution of PV with equivalent latitude (Butchart & Remsberg 1986; Nakamura 1995; Baldwin

& Dunkerton 1998; Liberato *et al.* 2007; Harvey *et al.* 2009), u_{ref} removes the effects of transient, reversible distortions to the PV field and hence underscores nonconservative effects. For example, NZ10ab use u_{ref} to diagnose the effects of mixing on the sharpening of jets in β-plane turbulence. It has been demonstrated by NS10 and NS11 that (the baroclinic generalization of) u_{ref} captures a greater seasonal variation and less high-frequency fluctuations than $\overline{u}$, suggesting that u_{ref} exhibits better signal-to-noise ratio as a climate diagnostic.

Thus the new diagnostic carries a flavor of Lagrangian-mean formalism by incorporating the material displacement with the contours of PV but avoids the difficulty of the GLM formalism by using equivalent latitude as a coordinate, which, unlike the center-of-mass latitude, is guaranteed to cover the entire globe uniformly even when the eddy amplitude is large. Moreover, as suggested by NZ10a, the global conservation of $A^* \cos\phi_e$ may be used to formulate the finite-amplitude (Lyapunov) stability theorems similar to those derived from the IC wave activity (McIntyre & Shepherd 1987; Shepherd 1988, 1989).

The purpose of this article is twofold. First, we shall theoretically relate A^* with the GLM pseudomomentum density and the IC wave activity by explicitly working out the formalisms for barotropic flow on the sphere. This will clarify that the three forms of wave activity satisfy similar conservation law of the form (1.3) but differ by the divergence of a vector, that is, they are related through a gauge transformation. Yet of the three only A^* satisfies the exact nonacceleration theorem for the zonal-mean flow $\bar{u}$. Second, we shall relate A^* quantitatively with the other more traditional measures of wave activity in a simple barotropic experiment on the sphere in which a jet is formed by localized wave forcing. This is a fundamental phenomenon of barotropic flow on a rotating sphere, investigated over the years analytically, experimentally and numerically (Kuo 1951; McEwan *et al.* 1980; Vallis 2006). The transport by waves results in a convergence of eastward momentum into the forcing region and westward momentum elsewhere. This is similar to the mechanism which maintains the midlatitude westerly winds against surface friction (Charney 1959; Eliassen & Palm 1961; Edmon *et al.* 1980; Boer & Shepherd 1983). Application of the different forms of wave activity to this controlled experiment clarifies the strengths and weaknesses of the diagnostics.

In the next two sections we will examine the theoretical connections among the GLM pseudomomentum density, the impulse-Casimir wave activity, and A^*. In §4 these measures of wave activity will be compared in the analysis of the numerical simulation of an eddy-driven jet. Sensitivity of these diagnostics to model truncation is also addressed. The final section provides a summary.

2. Circulation, wave activity, and Generalized Lagrangian Mean

In this section, we will examine the link between the new wave activity and the GLM pseudomomentum density by constructing a theory of the latter for barotropic flow on the sphere. To avoid the difficulty of Lagrangian mean coordinates located in the interior of the sphere (McIntyre 1980 §4.2), we will not derive the GLM set from the full 3D problem, but apply the GLM theory directly to the 2D barotropic vorticity equation on the sphere. Since the conservation of Kelvin's circulation is central to both the GLM theory and the novel construction of NZ10ab, NS10 and NS11, we will first outline the forms of circulation as well as the methods employed for its calculation.

2.1. *Circulation in the* (λ, μ)*-plane*

Consider a conservative, barotropic fluid motion on a sphere of radius a with rotation rate Ω. Since the motion is independent of height, we will work in the longitude-sine latitude coordinate $(\lambda, \mu) = (\lambda, \sin\phi)$, where ϕ is latitude. In these coordinates the area element of the fluid is given by

$$dS = a^2 \cos\phi d\lambda d\phi = a^2 d\lambda d\mu,$$

so the spherical surface is mapped onto a rectangular plane, which makes the kinematics similar to those in Cartesian coordinates. Note that the Eulerian fluid velocity is nondivergent

$$\mathbf{V} = (U, V) = (a\dot{\lambda}, a\dot{\mu}) \quad \text{and} \quad \partial U/\partial\lambda + \partial V/\partial\mu = 0,$$

where $U = u/\cos\phi$, $V = v\cos\phi$, and (u, v) are the velocities in the (λ, ϕ) coordinates. Here the dot (i.e. $\dot{\chi}$) indicates the material derivative of χ. The momentum equations in the (λ, μ)-plane are

$$\frac{D}{Dt}[U(1-\mu^2)] - 2\Omega\mu V = \frac{-1}{a}\frac{\partial p}{\partial\lambda} \tag{2.1}$$

$$\frac{D}{Dt}\left(\frac{V}{1-\mu^2}\right) + 2\Omega\mu U + \frac{\mu}{a}\left(U^2 - \frac{V^2}{(1-\mu^2)^2}\right) = \frac{-1}{a}\frac{\partial p}{\partial\mu}, \tag{2.2}$$

$$\text{where} \quad \frac{D}{Dt} = \frac{\partial}{\partial t} + \frac{U}{a}\frac{\partial}{\partial\lambda} + \frac{V}{a}\frac{\partial}{\partial\mu}$$

and p is pressure. Cross-differentiate (2.1) and (2.2) to obtain the vorticity equation

$$\frac{D}{Dt}\omega = 0, \qquad \omega(\lambda, \mu, t) = 2\Omega\mu + \frac{1}{a}\left\{\frac{\partial}{\partial\lambda}\left(\frac{V}{1-\mu^2}\right) - \frac{\partial}{\partial\mu}\left[U(1-\mu^2)\right]\right\}. \tag{2.3}$$

We express the Coriolis parameter $f = 2\Omega\mu$ in terms of a vector potential $\mathbf{A} = (a\Omega(1-\mu^2), 0, 0)$ so that $f = \mathbf{k}\cdot(\nabla\times\mathbf{A})$, where $\mathbf{k} = (0, 0, 1)$. Although a gradient vector of an arbitrary scalar field may be added to $\mathbf{A}$ without affecting the result, this particular choice ensures that Kelvin's circulation around the λ-periodic contour be defined correctly (Bühler 2009 §10). Then absolute vorticity ω can be written in terms of the curl of absolute velocity $\mathbf{V}^* + \mathbf{A}$

$$\mathbf{V}^* + \mathbf{A} \equiv \left((U + \Omega a)(1-\mu^2),\ \frac{V}{(1-\mu^2)}, 0\right) \equiv (M, N, 0), \tag{2.4}$$

$$\omega = \mathbf{k}\cdot(\nabla\times(\mathbf{V}^* + \mathbf{A})) = \frac{1}{a}\left(\frac{\partial}{\partial\lambda}N - \frac{\partial}{\partial\mu}M\right). \tag{2.5}$$

Now Kelvin's circulation C about a closed material contour can be expressed as

$$C = \oint(\mathbf{V}^* + \mathbf{A})\cdot d\mathbf{l} = \iint_D \omega dS, \tag{2.6}$$

where $d\mathbf{l}$ is the line element vector of the closed material contour and D denotes the domain enclosed by the contour. The last identity is due to the Stokes theorem. Kelvin's circulation is a conserved quantity for barotropic flow in the absence of forcing and dissipation. Since under that condition absolute vorticity is also material, we consider the circulation about these ω contours

$$C(\omega) = \iint_{\hat{\omega}\geqslant\omega} \hat{\omega} dS. \tag{2.7}$$

The surface integral of vorticity can be estimated easily from a gridded data set by weighted box counting. Simply determine if a given grid point is within the interior of a contour, then add the vorticity at that point times the area of the grid box, which is the spherical quadrangle at that latitude, $\Delta S_j = a^2 \cos\phi_j \Delta\phi\Delta\lambda$:

$$C(\omega) \simeq \sum_{\hat{\omega}_{ij} \geqslant \omega} \hat{\omega}_{ij} \Delta S_j, \tag{2.8}$$

where the subscripts (i, j) denote the longitudinal and latitudinal indices for the grid point. On the sphere there is an ambiguity about the definition of interior, so we have chosen the region designated by positive ω gradient pointing inward. This tends to be a connected region enclosing the north pole, however disconnected islands can occur and their contribution to the circulation should be included. Absolute circulation can also be expressed as a function of equivalent latitude. For a given value of absolute vorticity the corresponding equivalent latitude may be computed from the following relationship:

$$S(\omega) \equiv \iint\limits_{\hat{\omega} \geqslant \omega} dS = \int\limits_{\mu_e}^{1} 2\pi a^2 d\mu = 2\pi a^2 (1 - \mu_e) \simeq \sum_{\hat{\omega}_{ij} \geqslant \omega} \Delta S_j. \tag{2.9}$$

Absolute vorticity is a monotonic function of equivalent latitude by construction, and this function is invariant with time in the absence of dissipation and forcing. Hence $\omega(\mu_e)$ serves as a time-independent reference state, as does $C(\omega(\mu_e))$, which is at the core of the theory developed by NZ10a, NS10, and NS11. In reality (and in a numerical model) ω is not conserved exactly, but its contours provide a practical quasi-material coordinate which allows one to construct a continuously re-initialized version of the GLM theory (*modified Lagrangian mean*, McIntyre 1980).

2.2. *Generalized Lagrangian Mean pseudomomentum density*

Now we introduce the basic notions of GLM theory. For a more complete exposition the reader should refer to Andrews & McIntyre (1978*a*) and Bühler (2009). We start by constructing a one-to-one mapping between the particle locations on a zonal circle defined by $\mathbf{x} = (\lambda, \mu_m)$ and those on a wavy contour of ω, expressed as $\mathbf{x}+\boldsymbol{\xi} = (\lambda+\Delta\lambda, \mu_m+\Delta\mu)$ at a given time, where $\Delta\lambda(\lambda, \mu_m)$ and $\Delta\mu(\lambda, \mu_m)$ are the departure of the latter relative to the former. The Lagrangian zonal average along the contour and the corresponding eddy quantity for a scalar χ are defined as

$$\overline{\chi}^L(\mu_m, t) \equiv \frac{1}{2\pi} \int\limits_0^{2\pi} \chi(\lambda + \Delta\lambda, \mu_m + \Delta\mu, t) d\lambda. \tag{2.10}$$

$$\chi^l(\lambda, \mu_m, t) \equiv \chi(\lambda + \Delta\lambda, \mu_m + \Delta\mu, t) - \overline{\chi}^L(\mu_m, t). \tag{2.11}$$

Notice that the integral in (2.10) is defined with respect to the particle positions on the zonal circle at $\mu = \mu_m$, which are uniform in λ, but the distribution of the corresponding particles on the wavy contour is not necessarily uniform. Therefore (2.10) differs from an unweighted average along the wavy contour; rather it should be thought of as a thickness-weighted average over a wavy infinitesimal *tube* (McIntyre 1980)

$$\begin{aligned} \overline{\chi}^L &= \oint \tfrac{\chi}{|\nabla\omega|} dl \Big/ \oint \tfrac{dl}{|\nabla\omega|} \\ &= \tfrac{\partial}{\partial S} \iint\limits_{\hat{\omega} \geqslant \omega} \chi dS \approx \sum_{\omega+\Delta\omega \geqslant \hat{\omega}_{ij} \geqslant \omega} \chi_{ij} \Delta S_j \Big/ \sum_{\omega+\Delta\omega \geqslant \hat{\omega}_{ij} \geqslant \omega} \Delta S_j, \end{aligned} \tag{2.12}$$

where the circuit integrals are defined on the ω-contour and the last approximation is used to evaluate $\overline{\chi}^L$ from gridded data. Now if we require $\overline{\Delta\lambda} = \overline{\Delta\mu} = 0$ at $\mu = \mu_m$ so $\boldsymbol{\xi} = (\Delta\lambda, \Delta\mu)$ is an eddy quantity, then by substituting $\chi = \mu$ in (2.10) we have $\overline{\mu}^L = \mu_m$, which means that μ_m is the thickness-weighted average, or center-of-mass, latitude of the wavy material tube. Formulated this way, the material tendency of χ retains its exact structure upon Lagrangian averaging with no additional eddy terms.

$$\overline{\frac{D\chi}{Dt}}^L = \frac{\overline{D}^L}{Dt}\overline{\chi}^L = \left[\frac{\partial}{\partial t} + \frac{\overline{V}^L}{a}\frac{\partial}{\partial \mu}\right]\overline{\chi}^L, \tag{2.13}$$

where $\overline{V}^L = a\frac{\overline{D}^L}{Dt}\overline{\mu}^L$ is the Lagrangian-mean velocity with which the center-of-mass latitude moves. If an observed wavy ω-contour, whose Lagrangian-mean latitude is μ_m, had evolved from an eddy-free reference state conservatively, then the latitude of the contour in the reference state would have been μ_e. In this sense, the difference between μ_m and μ_e may be thought of as a (hypothetical) Stokes displacement of the contour associated with the eddies. Using (2.13), Kelvin's circulation theorem may be written as

$$\frac{\overline{D}^L}{Dt}C = \left[\frac{\partial}{\partial t} + \frac{\overline{V}^L}{a}\frac{\partial}{\partial \mu}\right]C = 0, \tag{2.14}$$

where C is defined in (2.6). We write out C using (2.4), (2.6) and the expression for the line element vector $d\mathbf{l} = a\left[\frac{\partial}{\partial\lambda}(\lambda + \Delta\lambda,\ \mu_m + \Delta\mu)\right]d\lambda$

$$\begin{aligned}
\tfrac{1}{2\pi a}C &= \tfrac{1}{a}\overline{(\mathbf{V}^* + \mathbf{A})\cdot(d\mathbf{l}/d\lambda)}^L \\
&= \overline{M(\lambda+\Delta\lambda, \mu_m+\Delta\mu)\tfrac{\partial(\lambda+\Delta\lambda)}{\partial\lambda}} + \overline{N(\lambda+\Delta\lambda, \mu_m+\Delta\mu)\tfrac{\partial(\mu_m+\Delta\mu)}{\partial\lambda}} \\
&= \overline{\left(\overline{M}^L + M^l\right)\left(1 + \tfrac{\partial(\Delta\lambda)}{\partial\lambda}\right) + \left(\overline{N}^L + N^l\right)\tfrac{\partial(\Delta\mu)}{\partial\lambda}} \\
&= \overline{M}^L + \overline{M^l\tfrac{\partial(\Delta\lambda)}{\partial\lambda} + N^l\tfrac{\partial(\Delta\mu)}{\partial\lambda}}.
\end{aligned}$$

The sum of the last two terms is defined as $-P(\mu_m, t)\cos\phi_m$, where P is the GLM (angular) pseudomomentum density. Thus

$$\frac{1}{2\pi a}C = \overline{M}^L - P(\mu_m)\cos\phi_m, \tag{2.15}$$

where the sign convention for the pseudomomentum density is standard. By applying the circulation theorem (2.14) to (2.15), we have

$$\frac{\overline{D}^L}{Dt}\overline{M}^L = \frac{\overline{D}^L}{Dt}\left(P(\mu_m)\cos\phi_m\right). \tag{2.16}$$

Thus, if P is steady following the center-of-mass latitude, there will be no acceleration of $\overline{M}^L$. This is an exact GLM nonacceleration theorem. Given (2.15) and that (1.9) can be also written as

$$\frac{1}{2\pi a}C = \overline{M}(\mu_e) + A^*(\mu_e)\cos\phi_e, \tag{2.17}$$

it is clear that the GLM and new formalisms differ only in the partition of Kelvin's circulation and that the conservation of circulation leads to the respective forms of nonacceleration theorem ((1.10) and (2.16)).

From (2.15) and (2.17),

$$-P(\mu_m)\cos\phi_m = A^*(\mu_e)\cos\phi_e + \overline{M}(\mu_e) - \overline{M}^L. \tag{2.18}$$

Thus the difference between $-P(\mu_m)\cos\phi_m$ and $A^*(\mu_e)\cos\phi_e$ amounts to the *Stokes*

correction to M relative to the zonal mean at equivalent latitude. Using (2.12) one can recast Lagrangian mean with respect to equivalent latitude

$$\overline{M}^L(\mu_e) = \frac{\partial}{\partial S}\iint\limits_{\hat{\omega}\geqslant\omega} M dS = -\frac{\partial}{\partial \mu_e}\left(\frac{1}{2\pi a^2}\iint\limits_{\hat{\omega}\geqslant\omega(\mu_e)} M dS\right) \equiv \frac{\partial L}{\partial \mu_e}, \tag{2.19}$$

whereas

$$\overline{M}(\mu_e) = -\frac{\partial}{\partial \mu_e}\left(\frac{1}{2\pi a^2}\iint\limits_{\mu\geqslant\mu_e} M dS\right) \equiv \frac{\partial Z}{\partial \mu_e}. \tag{2.20}$$

Therefore (2.18) becomes

$$-P(\mu_m)\cos\phi_m = A^*(\mu_e)\cos\phi_e + \frac{\partial}{\partial \mu_e}\left(Z - L\right). \tag{2.21}$$

Since $-P(\mu_m)\cos(\phi_m)$ and $A^*(\mu_e)\cos(\phi_e)$ differ by the divergence of a vector (in this case it only involves the derivative of a scalar with respect to equivalent latitude), the two may be linked to the same conservation law through *gauge transformation* (Held 1985; McIntyre & Shepherd 1987):

$$\frac{\partial}{\partial t}\left[A^*(\mu_e)\cos\phi_e\right] = \frac{\partial}{\partial \mu_e}\left[\overline{u'v'}(1-\mu_e^2)a^{-1}\right], \tag{2.22}$$

$$\frac{\partial}{\partial t}\left[-P(\mu_m)\cos\phi_m\right] = \frac{\partial}{\partial \mu_e}\left\{\left[\overline{u'v'}(1-\mu_e^2)a^{-1}\right] + \frac{\partial}{\partial t}\left(Z - L\right)\right\}, \tag{2.23}$$

where $-P(\mu_m)\cos(\phi_m)$, a property of the ω-contour, is treated as a function of μ_e and t. Equation (2.22) derives from (1.10) and (1.7). Since the right-hand sides of (2.22) and (2.23) vanish upon integration over μ_e, the global integral of both $-P(\mu_m)\cos\phi_m$ and $A^*(\mu_e)\cos\phi_e$ would be steady in the conservative limit. However, their meridional profiles are significantly different as we will see later: for example, $-P(\mu_m)\cos\phi_m$ is not sign-definite whereas $A^*(\mu_e)\cos\phi_e$ is. As shown below, the two quantities do not converge even at small amplitude.

2.3. *Small-amplitude theory*

Consider a slightly wavy ω-contour whose center-of-mass latitude is μ_m. The mapping between a point on the latitude circle $\mu = \mu_m$ and the corresponding point on the wavy contour is defined as

$$(\lambda, \mu_m) \rightarrow (\lambda, \Delta\lambda(\lambda, \mu_m), \mu_m + \Delta\mu(\lambda, \mu_m)), \tag{2.24}$$

where $\Delta\lambda$ and $\Delta\mu$ are $O(\alpha)$ and $\overline{\Delta\lambda} = \overline{\Delta\mu} = 0$. According to Andrews & McIntyre (1978*b*) the Stokes correction is defined as the difference between the Lagrangian mean around the ω-contour and the zonal mean, here evaluated at $\mu = \mu_m$

$$\chi^S = \overline{\chi}^L - \overline{\chi}(\mu_m) = \overline{\Delta\lambda\frac{\partial\chi'}{\partial\lambda}} + \overline{\Delta\mu\frac{\partial\chi'}{\partial\mu}} + \frac{1}{2}\overline{(\Delta\mu)^2}\frac{\partial^2\overline{\chi}}{\partial\mu^2} + O(\alpha^3). \tag{2.25}$$

Substitute $\chi = M$ and use the fact that $\partial\overline{M}/\partial\mu = -a\overline{\omega}$ to rewrite (2.25) as:

$$\begin{aligned}\overline{M}^L &= \overline{M}(\mu_m) + \overline{\Delta\lambda\tfrac{\partial M'}{\partial\lambda}} + \overline{\Delta\mu\tfrac{\partial M'}{\partial\mu}} + \tfrac{1}{2}\overline{(\Delta\mu)^2}\tfrac{\partial^2\overline{M}}{\partial\mu^2} + O(\alpha^3)\\ &= \overline{M}(\mu_m) + \overline{\Delta\lambda\tfrac{\partial M'}{\partial\lambda}} + \overline{\Delta\mu\tfrac{\partial M'}{\partial\mu}} - \tfrac{a}{2}\overline{(\Delta\mu)^2}\tfrac{\partial\overline{\omega}}{\partial\mu} + O(\alpha^3).\end{aligned} \tag{2.26}$$

In the small-amplitude limit the Lagrangian eddy terms may be approximated as

$$M^l = M' + \frac{\partial \overline{M}}{\partial \mu}\Delta\mu + O(\alpha^2), \quad \text{and} \quad N^l = N' + O(\alpha^2). \tag{2.27}$$

Substituting (2.27) into (2.15) we find that

$$\begin{aligned}
\tfrac{1}{2\pi a}C &= \overline{M}^L - P(\mu_m)\cos\phi_m = \overline{M}(\mu_m) + M^S - P(\mu_m)\cos\phi_m \\
&= \overline{M}(\mu_m) + \overline{\Delta\lambda \tfrac{\partial M'}{\partial \lambda}} + \overline{\Delta\mu \tfrac{\partial M'}{\partial \mu}} - \tfrac{a}{2}\overline{(\Delta\mu)^2}\tfrac{\partial \overline{\omega}}{\partial \mu} \\
&\quad + \overline{\left(M' + \tfrac{\partial \overline{M}}{\partial \mu}\Delta\mu\right)\tfrac{\partial(\Delta\lambda)}{\partial\lambda}} + \overline{N'\tfrac{\partial(\Delta\mu)}{\partial\lambda}} + O(\alpha^3) \\
&= \overline{M}(\mu_m) + \overline{\Delta\mu\left(\tfrac{\partial M'}{\partial\mu} - \tfrac{\partial N'}{\partial\lambda}\right)} - \tfrac{a}{2}\overline{(\Delta\mu)^2}\tfrac{\partial\overline{\omega}}{\partial\mu} - \tfrac{1}{2}\tfrac{\partial\overline{M}}{\partial\mu}\tfrac{\partial\overline{(\Delta\mu)^2}}{\partial\mu} + O(\alpha^3) \\
&= \overline{M}(\mu_m) - a\overline{\Delta\mu\omega'} - \tfrac{a}{2}\overline{(\Delta\mu)^2}\tfrac{\partial\overline{\omega}}{\partial\mu} - \tfrac{1}{2}\tfrac{\partial\overline{M}}{\partial\mu}\tfrac{\partial\overline{(\Delta\mu)^2}}{\partial\mu} + O(\alpha^3).
\end{aligned} \tag{2.28}$$

To get from line 1 to line 2 in the above, we have used (2.26). From line 2 to 3 we have used integration by parts, $\partial(\Delta\lambda)/\partial\lambda + \partial(\Delta\mu)/\partial\mu = O(\alpha^2)$, and from line 3 to 4, (2.5). Since in the small-amplitude limit $\omega' = -(\partial\overline{\omega}/\partial\mu)\Delta\mu + O(\alpha^2)$, the above can be further rendered as

$$\frac{1}{2\pi a}C = \overline{M}(\mu_m) + \left.\frac{a}{2}\overline{(\Delta\mu)^2}\frac{\partial\overline{\omega}}{\partial\mu}\right|_{\mu=\mu_m} - \left.\left(\frac{1}{2}\frac{\partial\overline{M}}{\partial\mu}\frac{\partial\overline{(\Delta\mu)^2}}{\partial\mu}\right)\right|_{\mu=\mu_m} + O(\alpha^3). \tag{2.29}$$

Now the small amplitude limit of A^* is (NS10 appendix)

$$A^*(\mu_e) = \frac{a}{2\cos\phi_e}\overline{(\Delta\mu_e)^2}\left.\frac{\partial\overline{\omega}}{\partial\mu}\right|_{\mu=\mu_e} + O(\alpha^3), \tag{2.30}$$

where $\Delta\mu_e$ is the *normal* displacement of the contour from the zonal circle $\mu = \mu_e$. It is easy to show that the difference between μ_m and μ_e as well as those between $\Delta\mu$ and $\Delta\mu_e$ are $O(\alpha^2)$, hence the difference between the second term on the right-hand side of (2.29) and $A^*(\mu_e)\cos\phi_e$ is at most $O(\alpha^3)$. Thus (2.29) becomes

$$\frac{1}{2\pi a}C = \overline{M}(\mu_m) + A^*(\mu_e)\cos\phi_e - \frac{1}{2}\left.\left(\frac{\partial\overline{M}}{\partial\mu}\frac{\partial\overline{(\Delta\mu)^2}}{\partial\mu}\right)\right|_{\mu=\mu_m} + O(\alpha^3). \tag{2.31}$$

Alternatively,

$$\frac{1}{2\pi a}C = \overline{M}\left(\mu_m - \frac{1}{2}\left.\frac{\partial\overline{(\Delta\mu)^2}}{\partial\mu}\right|_{\mu=\mu_m}\right) + A^*(\mu_e)\cos\phi_e + O(\alpha^3). \tag{2.32}$$

Equation (2.32) is a small-amplitude limit of (2.17) provided that

$$\mu_e = \mu_m - \frac{1}{2}\left.\frac{\partial\overline{(\Delta\mu)^2}}{\partial\mu}\right|_{\mu=\mu_m} + O(\alpha^3). \tag{2.33}$$

Thus (2.33) defines the Stokes displacement $\mu_m - \mu_e$ and the Lagrangian time derivative of (2.33) defines the Lagrangian-mean velocity:

$$\frac{\overline{D}^L}{Dt}(\mu_m - \mu_e) = \frac{\overline{D}^L}{Dt}\mu_m = \frac{\overline{V}^L}{a} = \frac{\partial}{\partial t}\left.\left(\frac{1}{2}\frac{\partial\overline{(\Delta\mu)^2}}{\partial\mu}\right)\right|_{\mu=\mu_m} + O(\alpha^3). \tag{2.34}$$

By taking the time derivative of (2.29) at a fixed μ and observing that the tendency of the mean quantities is $O(\alpha^2)$

$$\begin{aligned} \tfrac{\partial}{\partial t}\left(\tfrac{C}{2\pi a}\right) &= \tfrac{\partial \overline{M}}{\partial t} + \tfrac{\partial \overline{\omega}}{\partial \mu}\tfrac{\partial}{\partial t}\left(\tfrac{a\overline{(\Delta\mu)^2}}{2}\right) - \tfrac{\overline{V}^L}{a}\tfrac{\partial \overline{M}}{\partial \mu} + O(\alpha^3) \\ &= \tfrac{\partial \overline{M}}{\partial t} + \tfrac{\partial \overline{\omega}}{\partial \mu}\tfrac{\partial}{\partial t}\left(\tfrac{a\overline{(\Delta\mu)^2}}{2}\right) - \tfrac{\overline{V}^L}{a}\tfrac{\partial}{\partial \mu}\left(\tfrac{C}{2\pi a}\right) + O(\alpha^3) \end{aligned} \tag{2.35}$$

where the last line used $C = 2\pi a\overline{M} + O(\alpha^2)$ and $\overline{V}^L = O(\alpha^2)$. Thus,

$$\left(\frac{\partial}{\partial t} + \frac{\overline{V}^L}{a}\frac{\partial}{\partial \mu}\right)\left(\frac{C}{2\pi a}\right) = \frac{\partial}{\partial t}\overline{M} + \frac{\partial \overline{\omega}}{\partial \mu}\frac{\partial}{\partial t}\left(\frac{a\overline{(\Delta\mu)^2}}{2}\right) + O(\alpha^3). \tag{2.36}$$

Since

$$\frac{\partial \overline{M}}{\partial t} = \overline{V'\omega'} \quad \text{and} \quad \frac{\partial \overline{\omega}}{\partial \mu}\frac{\partial}{\partial t}\left(\frac{a\overline{(\Delta\mu)^2}}{2}\right) = -\overline{V'\omega'} + O(\alpha^3),$$

(2.36) leads to the small-amplitude limit of Kelvin's circulation theorem

$$\left(\frac{\partial}{\partial t} + \frac{\overline{V}^L}{a}\frac{\partial}{\partial \mu}\right)C = \frac{\overline{D}^L}{Dt}C = O(\alpha^3). \tag{2.37}$$

Now comparing (2.31) and the second identity of (2.28)

$$\begin{aligned} -P(\mu_m)\cos\phi_m &= A^*(\mu_e)\cos\phi_e - \tfrac{1}{2}\left(\tfrac{\partial \overline{M}}{\partial \mu}\tfrac{\partial \overline{(\Delta\mu)^2}}{\partial \mu}\right)\Big|_{\mu=\mu_m} - M^S + O(\alpha^3) \\ &= A^*(\mu_e)\cos\phi_e + \overline{M}(\mu_e) - \overline{M}(\mu_m) - M^S + O(\alpha^3) \\ &= A^*(\mu_e)\cos\phi_e + \overline{M}(\mu_e) - \overline{M}^L + O(\alpha^3). \end{aligned} \tag{2.38}$$

This is the small-amplitude limit of (2.18). Since (using (2.28) and integral by parts etc.)

$$\begin{aligned} -\tfrac{1}{2}\left(\tfrac{\partial \overline{M}}{\partial \mu}\tfrac{\partial \overline{(\Delta\mu)^2}}{\partial \mu}\right)\Big|_{\mu=\mu_m} &= \tfrac{a\overline{\omega}}{2}\tfrac{\partial \overline{(\Delta\mu)^2}}{\partial \mu} = \tfrac{\partial}{\partial \mu}\left[\tfrac{a\overline{\omega}}{2}\overline{(\Delta\mu)^2}\right] - \tfrac{a}{2}\tfrac{\partial \overline{\omega}}{\partial \mu}\overline{(\Delta\mu)^2} \\ &= \tfrac{\partial}{\partial \mu}\left[\tfrac{a\overline{\omega}}{2}\overline{(\Delta\mu)^2}\right] + M^S - \overline{\Delta\lambda\tfrac{\partial M'}{\partial \lambda}} - \overline{\Delta\mu\tfrac{\partial M'}{\partial \mu}} + O(\alpha^3) \\ &= \tfrac{\partial}{\partial \mu}\left[\tfrac{a\overline{\omega}}{2}\overline{(\Delta\mu)^2}\right] + M^S + \overline{\tfrac{\partial(\Delta\lambda)}{\partial \lambda}M'} - \overline{\Delta\mu\tfrac{\partial M'}{\partial \mu}} + O(\alpha^3) \\ &= \tfrac{\partial}{\partial \mu}\left[\tfrac{a\overline{\omega}}{2}\overline{(\Delta\mu)^2}\right] + M^S - \overline{\tfrac{\partial(\Delta\mu)}{\partial \mu}M'} - \overline{\Delta\mu\tfrac{\partial M'}{\partial \mu}} + O(\alpha^3) \\ &= \tfrac{\partial}{\partial \mu}\left[\tfrac{a\overline{\omega}}{2}\overline{(\Delta\mu)^2} - \overline{M'\Delta\mu}\right] + M^S + O(\alpha^3), \end{aligned}$$

(2.38) may be further rewritten as

$$-P(\mu_m)\cos\phi_m = A^*(\mu_e)\cos\phi_e + \frac{\partial}{\partial \mu}\left[\frac{a\overline{\omega}}{2}\overline{(\Delta\mu)^2} - \overline{M'\Delta\mu}\right] + O(\alpha^3). \tag{2.39}$$

This is the small-amplitude version of (2.21) and again the difference between $-P(\mu_m)\cos\phi_m$ and $A^*(\mu_e)\cos\phi_e$ is written in terms of the divergence of a vector, linking the former to the E-P theorem through gauge transformation ((2.23)). Yet since all three terms in (2.39) are $O(\alpha^2)$, $-P(\mu_m)\cos\phi_m$ and $A^*(\mu_e)\cos\phi_e$ do not converge even at the small-amplitude limit.

3. Impulse-Casimir wave activity

As the conservation of Kelvin's circulation leads directly to the nonacceleration theorem involving the GLM pseudomomentum, the conservation of Kelvin's impulse has been exploited to construct another class of eddy metrics. The measure of local wave activity

introduced by Killworth & McIntyre (1985) is based on the impulse-Casimir method and can be defined as

$$A_{IC}(\omega_R, \omega_\epsilon)\cos\phi = -a\mu\omega_\epsilon + I(\omega_R + \omega_\epsilon) - I(\omega_R), \tag{3.1}$$

where $\omega_R(\mu)$ is a zonally symmetric, time-independent reference state of absolute vorticity and $\omega_\epsilon(\lambda, \mu, t) = \omega(\lambda, \mu, t) - \omega_R(\mu)$ is the departure from that reference state. (Note that generally $\omega_\epsilon \neq \omega' = \zeta'$ since the former may contain a nonzero zonal-mean component.) McIntyre & Shepherd (1987) show that the above construction is based on the conservation of the density of Kelvin's impulse $\mu\omega$ and the impulse-Casimir function

$$I(\omega) = \int_{\omega_{min}}^{\omega} a\mu_R(\tilde{\omega})d\tilde{\omega}. \tag{3.2}$$

Here ω_{min} is the minimum value of ω_R and $\mu_R(\omega)$ is the inverse of $\omega_R(\mu)$, where we assume that ω_R is a monotonic function of μ so that its inverse is uniquely defined. For example, if the reference state is chosen to be solid body rotation $\omega_R = 2\Omega\mu$, then the density of IC wave activity may be written as

$$A_{IC}(\lambda, \mu, t)\cos\phi = \frac{1}{2}a(\omega_\epsilon)^2/(2\Omega). \tag{3.3}$$

This provides a two-dimensional distribution of wave activity density on the sphere. In contrast, A_L, A^*, and P do not provide any information about the longitudinal distribution. To facilitate the comparison, we will take the zonal average of A_{IC}. As shown by McIntyre & Shepherd (1987), in the small-amplitude limit

$$A_{IC}(\lambda, \mu, t)\cos\phi = \frac{a}{2}\frac{\zeta'^2}{d\omega_R/d\mu} + O(\alpha^3), \tag{3.4}$$

so the zonal average of (3.4) is identical with (1.4). Therefore, $\overline{A_{IC}}$ converges to A_L (and thus A^*) at small amplitude. As shown by Killworth & McIntyre (1985), A_{IC} satisfies a local flux conservation. Its zonally averaged form is

$$\frac{\partial}{\partial t}\{\overline{A_{IC}}\cos\phi\} = \frac{\partial}{\partial\mu}\left[a^{-1}(1-\mu^2)\left(\overline{u'v'} - \overline{v'A_{IC}}\right)\right], \tag{3.5}$$

where we used $v_\epsilon = v'$ and $\overline{u_\epsilon v_\epsilon} = \overline{u'v'}$ for the barotropic flow. Equation (3.5) differs from (2.22) by the last term in the right-hand side. This term denotes the eddy advection of wave activity, which corresponds to the $O(\alpha^3)$ term on the right-hand side of (1.5) in the small-amplitude limit. This advective flux term may be eliminated through an implicit gauge transformation

$$\overline{A_{IC}} \to \overline{A_{IC}}^* \equiv \overline{A_{IC}} + \frac{1}{\cos\phi}\int_{t_0}^{t}\frac{\partial}{\partial\mu}\left[a^{-1}(1-\mu^2)\overline{v'A_{IC}}\right]d\tilde{t}. \tag{3.6}$$

Now we see that the tendency of this transformed wave activity is just the E-P flux convergence

$$\frac{\partial}{\partial t}\{\overline{A_{IC}}^*\cos\phi\} = \frac{\partial}{\partial\mu}\left[\overline{u'v'}(1-\mu^2)a^{-1}\right]. \tag{3.7}$$

Comparing with (2.22), we see that $A^* = \overline{A_{IC}}^*$ for all time if it is true at one time. Thus, like P, $\overline{A_{IC}}$ is also related to A^* through gauge transformation. However, only A^* satisfies the exact nonacceleration theorem for $\bar{u}$ (1.10). Since the right-hand side of

(3.5) vanishes in the domain average, the global integral of $\overline{A_{IC}}\cos\phi$ is steady under the conservative dynamics, even if its meridional profile is unsteady.

4. A numerical experiment

In this section we will conduct an idealized numerical experiment, in which an eddy forcing is applied to drive a zonal jet on the rotating sphere. We will then use the result of the experiment as a controlled test bed for the various forms of wave activity diagnostics introduced earlier. The vorticity equation (2.3) can be written in terms of a streamfunction ψ since (U, V) is nondivergent:

$$\frac{\mathrm{D}\omega}{\mathrm{D}t} = \frac{\partial\omega}{\partial t} + \frac{1}{a^2}\left(\frac{\partial\psi}{\partial\lambda}\frac{\partial\omega}{\partial\mu} - \frac{\partial\psi}{\partial\mu}\frac{\partial\omega}{\partial\lambda}\right) = Q, \tag{4.1}$$

where Q represents forcing and dissipation. This equation is discretized with a standard spectral transform method truncated at T85 on a 256×128 Gaussian grid. The size and the rotation rate of the sphere are chosen to be those of the earth. The time-stepping is done with an Adams-Bashforth third-order scheme and a time step of eight minutes. A 6th-order hyperviscosity is applied that damps the highest order modes with an e-folding timescale of one day (Durran 2010 §6).

To simulate midlatitude stirring by planetary waves, a meridionally localized, stationary vorticity forcing is applied to a fluid initially in solid body rotation. The forcing is slowly increased then maintained at a constant amplitude for thirty days after which it is slowly reduced and the system is allowed to evolve freely for another thirty days. The forcing has a Gaussian profile in latitude, centered at 45°N with a width of 20 degrees and sinusoidal, wavenumber four amplitude in the longitudinal direction. The maximum amplitude of the forcing is $2.5\times10^{-10}s^{-2}$ which is found to produce a reasonable amount of stirring without generating barotropic instability early in the experiment as to obscure the wave dynamics. The specific form of Q is

$$Q = \gamma_\zeta + \kappa\nabla^6\omega$$

$$\text{where } \gamma_\zeta(\lambda,\mu,t) = \begin{cases} \gamma_0(t)10^{-((\mu-1/\sqrt{2})/.24)^2}\cos(4\lambda) & 35^\circ \leqslant \phi \leqslant 55^\circ \\ 0 & |\phi - 45^\circ| > 10^\circ, \end{cases}$$

where the shape of γ_0 is sketched in figure 3b below. Because of this nonconservative term, (1.10) is modified to

$$\frac{\partial}{\partial t}A^* = -\overline{v'\zeta'} + F + D, \qquad \frac{\partial}{\partial t}u_{ref} = \frac{\partial}{\partial t}(\bar{u} + A^*) \approx F + D, \tag{4.2}$$

where F and D stand for forcing and dissipation of wave activity, respectively. The dissipation of wave activity is due to diffusive flux (mixing) of vorticity and always negative (NZ10a). Note that u_{ref} is driven solely by nonconservative processes. Hyperdiffusion of $\bar{u}$ also affects u_{ref} but this effect is small and ignored. The zonal-mean flow $\bar{u}$ is not directly driven by the external forcing; rather wave activity is spun up first and subsequent decay through eddy vorticity flux drives the flow

$$\frac{\partial\overline{u}}{\partial t} = \overline{v'\zeta'} = -\frac{1}{a\cos\phi}\frac{\partial}{\partial\mu}\left(\overline{u'v'}(1-\mu^2)\right). \tag{4.3}$$

The last term is the eddy momentum flux convergence, or equivalently the E-P flux divergence, arising from (1.7).

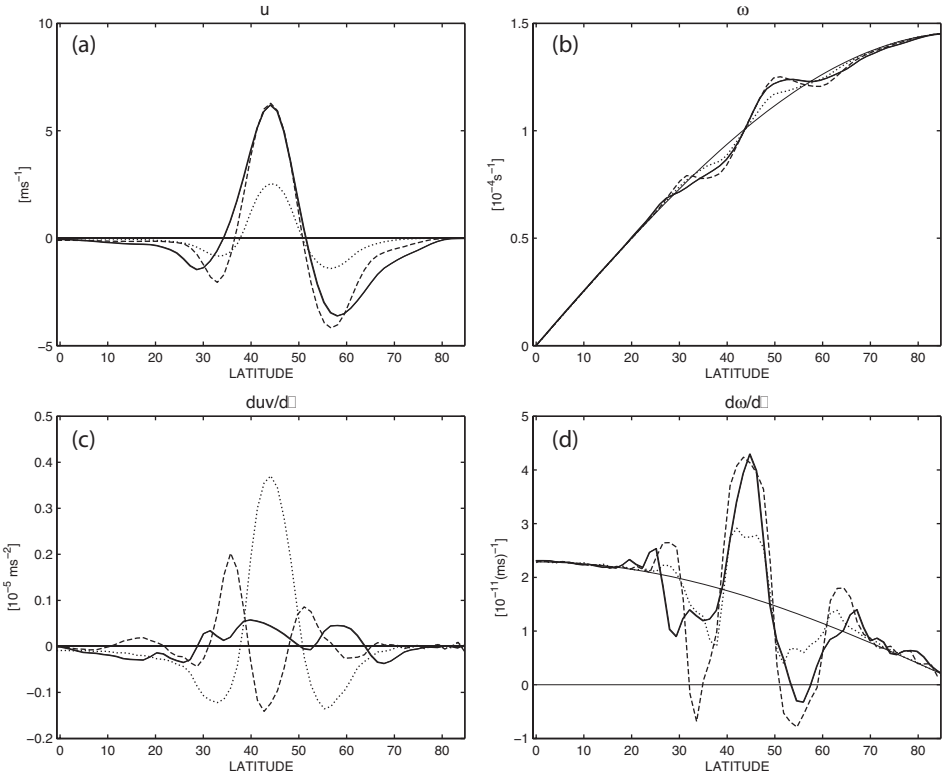

FIGURE 1. Zonal-mean fields in the Northern Hemisphere averaged over three twenty-day periods of the simulation. (a) zonal wind $\overline{u}$, (b) absolute vorticity $\overline{\omega}$, (c) eddy momentum flux convergence, and (d) the gradient of $\overline{\omega}$. Averages are taken for first twenty days (dot), days 25-44 (dash) and last twenty days (solid). Initial profiles for each quantity are also plotted as solid curves.

4.1. *Mean flow, wave activity, and reference state*

The formation of a jet is illustrated in figure 1a with profiles of the zonal mean wind averaged over three twenty-day intervals. Westerlies localized in the region of forcing develop progressively throughout the simulation with easterlies on both flanks. The asymmetry in the easterlies is pronounced with broader and stronger westward flow on the poleward side of the jet. As the jet emerges, finite-amplitude cyclone/anti-cyclone pairs propagate away from the forcing region (not shown). The associated perturbation to the initial distribution of planetary vorticity is seen in figure 1b. Within the first twenty days a large positive gradient in $\overline{\omega}$ develops at the axis of the jet, with reversals in the gradient in the regions of westward flow (figures 1b,d). These negative gradients lead to barotropic instability which produces strong mixing on the flanks of the jet. Figure 1c indicates large convergence of momentum into the axis of the jet early in the simulation with a symmetric pattern of divergence on the flanks. Later in the experiment this symmetry is broken, giving way to a more complex pattern of eddy forcing. This results in the evolution of the zonal-mean wind beyond the termination of the forcing and even continuing at the end of the integration.

To illustrate the nonconservative modification of the mean state, we show in figure 2 $u_{ref}(\phi_e)$ and $\omega(\phi_e)$, to be compared with $\overline{u}(\phi)$ and $\overline{\omega}(\phi)$ in figure 1. As noted in (4.2) and by NZ10ab, these quantities evolve only in response to forcing and mixing, and the

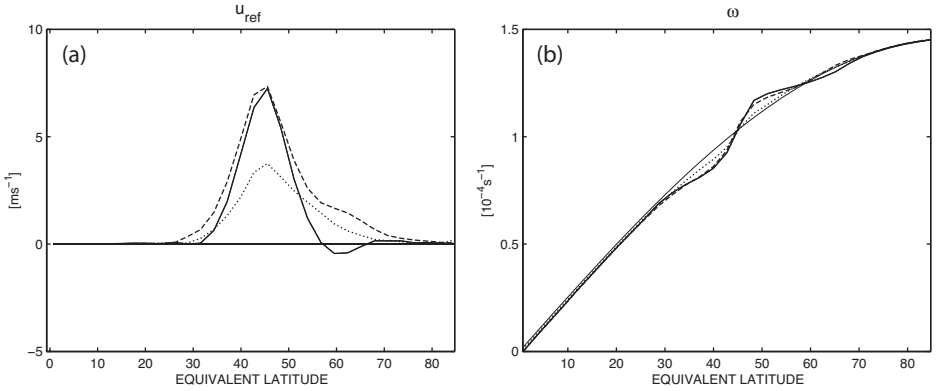

FIGURE 2. (a) $u_{ref}(\phi_e)$ in the Northern Hemisphere averaged over the same three, twenty-day intervals as in figure 1. (b) $\omega(\phi_e)$, the distribution of absolute vorticity with equivalent latitude, also averaged over the same twenty day intervals.

difference with the zonal-mean quantities largely reflects the eddy-mean flow interaction through the E-P flux divergence. The tendency of u_{ref} due to mixing (D in (4.2)) is always negative, as the diffusive flux of vorticity acts as a damping on A^*.

It is seen that u_{ref} (figure 2a) is greater in magnitude than $\overline{u}$ in figure 1a throughout the domain during each interval. This reflects $u_{ref} = \overline{u} + A^*$ and $A^* \geqslant 0$. u_{ref} attains its maximum of more than $8.0ms^{-1}$ before day 25 and remains fairly constant near the jet axis after about day 40. The gain in u_{ref} is due to forcing (F in (4.2)), and it extends beyond the region of forcing into high equivalent latitudes (dotted and dashed curves in figure 2a). This is because the waviness in absolute vorticity allows high-equivalent-latitude fluid to migrate into the forcing region. The main evolution of u_{ref} after initial growth is a progressive narrowing of the jet as A^* is dissipated on the flanks, reflected in the decrease in u_{ref} from the dashed- to solid curve, with greater dissipation occurring on the poleward side. The profile of absolute vorticity in figure 2b remains (by construction) a monotonic function of equivalent latitude, but it shows an irreversible change in gradients as a result of forcing and mixing. In particular, the enhanced mixing at the flanks of the jet markedly reduce the gradients there, reinforcing the strong gradient at the jet axis and producing a staircase-like profile (Dritschel & McIntyre 2008; NZ10b).

The E-P flux divergence governs the tendency of both $\overline{u}$ and A^*, however without wave activity their relative magnitude is unknown. In figure 3 we compare this standard flux-based analysis of wave forcing with a direct assessment of wave activity, averaged within the forcing region (35-55°N). As seen in figure 3a, the E-P flux divergence (dashed line) is positive for the first 27 days and the zonal-mean flow (solid line) increases within the forcing region. After that point barotropic instability ensues due to the vanishing of the absolute vorticity gradient and the E-P flux divergence begins to oscillate, whilst $\overline{u}$ slowly continues to grow for the duration of the simulation.

In figure 3b the evolution of the reference state flow u_{ref} (solid line) and wave activity A^* (dashed line) within the forcing region are plotted. Since $u_{ref}(\phi_e, t) = \overline{u} + A^*$, these curves represent the partitioning of u_{ref} into eddy and zonal-mean components. Initially u_{ref} grows rapidly and this is almost entirely due to the growth of wave activity through forcing. The two curves only start to diverge around day 9, when $\overline{u}$ becomes significant. After about day 12 wave activity equilibrates and starts to oscillate until the end of the forcing period around day 40. The initial equilibration is due to the balance between the gain through forcing and the loss through E-P flux convergence, but the subsequent

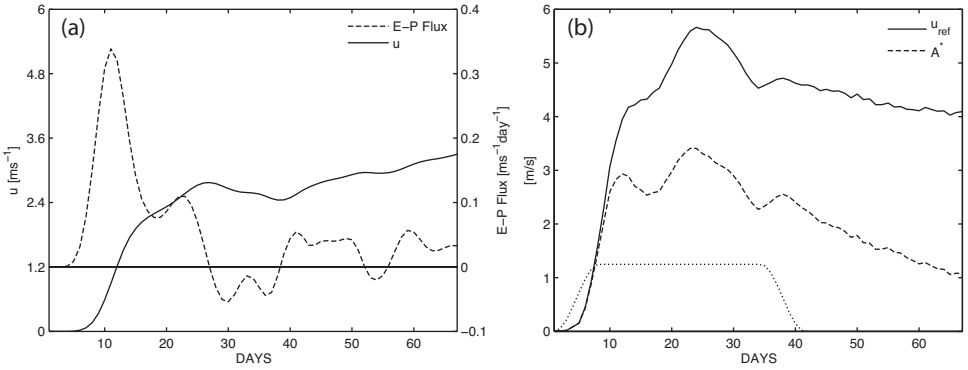

FIGURE 3. (a) Zonal-mean zonal wind (solid line) and E-P flux divergence (dashed line), averaged within the forcing region (35-55°N) as a function of time in days. (b) u_{ref} (solid line) and wave activity density (dashed line) also averaged over the forcing region. The dotted line shows the timing of forcing, with a maximum amplitude of $2.5 \times 10^{-10} s^{-2}$ and a minimum of zero.

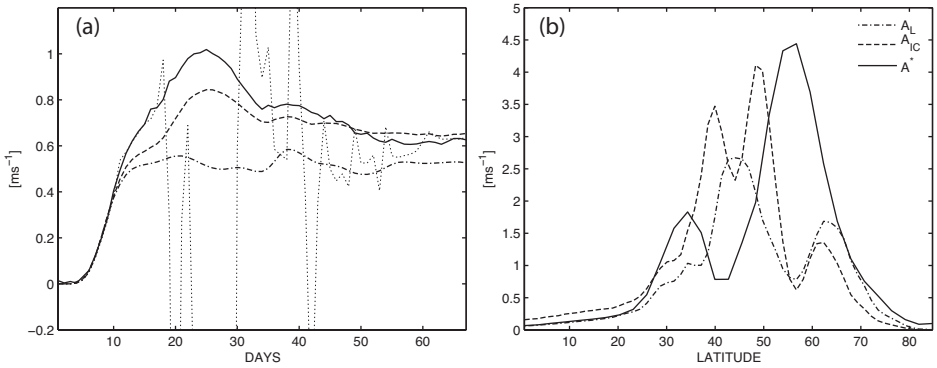

FIGURE 4. (a) Global-mean wave activities (in ms^{-1}) for the jet simulation as a function of time: linear wave activity A_L (dot-dashed), finite-amplitude impulse-Casimir wave activity $\overline{A_{IC}}$(dashed) and A^* (solid). Dotted line represents A_L calculated with instantaneous gradient of zonal-mean absolute vorticity. (b) Time-averaged (days 0-67) wave activities as functions of latitude using the same line markers as in (a). Note that the coordinate for A^* is equivalent latitude.

oscillation is also affected by dissipation due to mixing. The reference-state flow u_{ref} equilibrates much later ($\approx$ day 24) as the forcing is balanced by the dissipation. After the forcing has been turned off wave activity steadily declines until the end of the simulation. A significant fraction of this decline is due to conversion to $\overline{u}$ through the E-P flux convergence, evident in the increase in $\overline{u}$ in figure 3a. In comparison, u_{ref} decreases much more slowly than A^*. The decrease in u_{ref} in this freely evolving stage primarily reflects the dissipation of wave activity due to mixing. The increasing $\overline{u}$ and decreasing A^* boosts the fraction of the former in u_{ref} toward the end of the simulation, making the flow less wavy, although A^* is greater than $\overline{u}$ until the forcing is turned off. Such assessment of the eddy-mean partitioning of momentum is not accessible through the E-P flux analysis alone.

4.2. *Wave activity comparison*

We have seen that A^* can provide additional insight for interpreting an evolving flow. Now we compare it with other forms of wave activity using the same result of the above

simulation. In figure 4a the time dependence of the global-mean A^* is shown (solid curve), together with finite-amplitude impulse-Casimir wave activity $\overline{A_{IC}}$ (dashed) and the wave activity of the linearized problem, A_L (dot-dashed). We use (1.4) to define A_L, by taking the initial condition (solid body rotation with no wind) as the reference state $d\omega_R/d\mu = 2\Omega$, and remove the zonal-mean component from ζ'. We also use the same reference state for $\overline{A_{IC}}$. The three curves overlap until about day 10, which confirms their convergence in the small-amplitude limit. After that they begin to diverge from one another. The linear wave activity A_L remains smaller in amplitude than the others, while the two finite-amplitude measures depict wave growth until day 24 when barotropic instability begins to alter the flow. At day 24, the global-mean $\overline{A_{IC}}$ and A_L are roughly 80 and 50 percent of A^*, respectively. During the final twenty days A_{IC} and A^* show good agreement and remain fairly constant as would be expected in the absence of forcing. The discrepancy between the global-mean A^* and $\overline{A_{IC}}$ is primarily due to the nonconservative alteration of the reference state. Although identical initially, the reference state for A^* evolves due to forcing and mixing, whereas the reference state for $\overline{A_{IC}}$ is fixed in time.

Comparing (1.4) and (3.3) it is clear that the difference between A_L and $\overline{A_{IC}}$ is due to the contribution from $\overline{\omega_\epsilon}^2/2\Omega$, namely the part of $\overline{A_{IC}}$ associated with the zonal-mean component of ω_ϵ spun up by the eddy-mean flow interaction. Therefore as a comparison, we show the wave activity linearized about the instantaneous gradient of zonal-mean absolute vorticity (i.e., replace $d\omega_R/d\mu$ in (1.4) by $\partial\overline{\omega}/\partial\mu$) in the dotted curve. This linear diagnostic reproduces A^* remarkably well until about day 16, much longer than A_L or even $\overline{A_{IC}}$, suggesting the importance of flow profiles for computing wave activity accurately. However, this measure of wave activity lacks conservation properties of A_L or $\overline{A_{IC}}$ and breaks down as soon as $\partial\overline{\omega}/\partial\mu$ vanishes due to stirring by eddies, which causes the wild oscillation after day 16.

In figure 4b the time averaged distribution of wave activity with latitude shows several important differences between these three diagnostics. The linear measure A_L indicates a maximum in wave activity at the center of the forcing region, while the two finite-amplitude measures exhibit local minima there. The intriguing distinction between $\overline{A_{IC}}$ and A^* is that one indicates a more focused, symmetric distribution with respect to the jet, while the other shows a pronounced maximum on the poleward side of the forcing region.

The comparison is further substantiated by figure 5, in which the meridional profiles of A^*, $\overline{A_{IC}}$ and A_L are plotted as functions of time. Each measure shows the tendency of wave activity to split into a subtropical and subpolar tracks, similar to the barotropic decay of pseudomomentum observed in Held & Phillips (1987). Only A^* shows a clear separation of the two tracks with a persistent minimum in between, where the flow is accelerated. Also A^* exhibits greater amplitude and broader extent in the poleward branch, consistent with the enhanced deceleration observed in that region (figure 5a). In contrast, $\overline{A_{IC}}$ shows two narrow tracks on the poleward side of the jet, the main track near the axis and a weaker track in higher latitudes (figure 5b). Thus, despite the similar behaviors in the global mean (figure 4a), A^* and $\overline{A_{IC}}$ show substantial differences in their meridional profiles. The differences are largely due to the nonlocal nature of equivalent latitude, which absorbs the flux of wave activity in (3.5). A^* is more closely related to the mean flow modification shown in figure 1a than $\overline{A_{IC}}$. The linear wave activity A_L shows similarity to $\overline{A}_{IC}$ in the early stage of evolution and in the secondary track in high latitudes (figure 5b,c). However, A_L does not reproduce the strong signals on the immediate flanks of the jet in $\overline{A}_{IC}$ around days 18-40, implying that they are largely due to mean flow modification. Because A_L lacks these signals on both sides of the jet axis, its time-mean profile in figure 4b shows maximum, not minimum, at the jet axis.

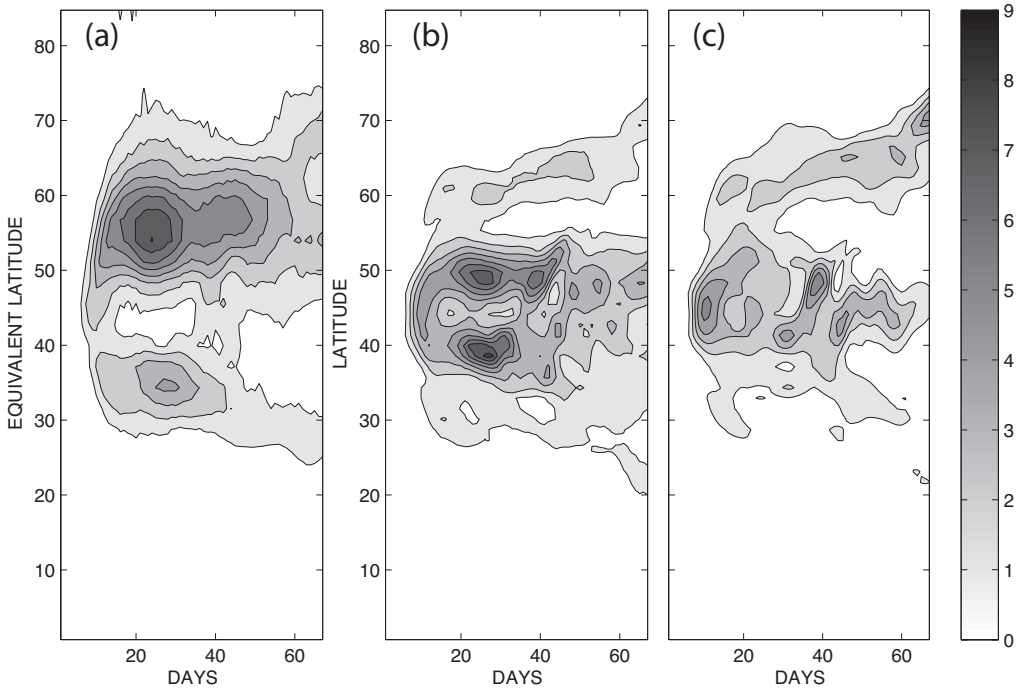

FIGURE 5. Time-latitude diagrams for three wave activity measures. (a) Wave activity A^* as a function of time and equivalent latitude. (b) The zonally averaged A_{IC} as a function of time and latitude. (c) Same as (b) but for A_L. All panels are plotted with the same grayscale, with a contour interval of 1 ms^{-1}.

In figure 6 we also compare $A^* \cos\phi_e$ with the GLM pseudomomentum density $-P\cos\phi_m$. First, we plot equivalent latitude μ_e (figure 6a) and the center-of-mass latitude μ_m (figure 6b) for ω-contours in the Northern Hemisphere as a function of time and the value of ω. The center-of-mass latitude is computed using (2.12) with $\chi_{ij} = \mu_j$. Both μ_e and μ_m are initially linear with ω, but the contours of μ_e quickly spreads in the forcing region. This is consistent with the *increase* in $\partial\omega/\partial\mu_e$ in the same region (figure 2b), due to forcing and mixing (without these nonconservative effects, $\mu_e(\omega)$ would be time-independent). Yet by construction μ_e remains a monotonic function of ω. In contrast, the evolution of μ_m is more complicated: the divergence and convergence of its contours do not necessarily coincide with those of the μ_e-contours, and there are some small 'islands,' implying that $\omega(\mu_m)$ can be locally multi-valued. This is a well-known difficulty in the GLM analysis, and for this reason we will not use μ_m as the coordinate for $-P\cos\phi_m$ but use ω instead. $-P\cos\phi_m$ is computed as the difference between $C/2\pi a$ and $\overline{M}^L$ using (2.15).

Wave activity $A^*\cos\phi_e$ shown in figure 6d essentially duplicates figure 5a with the $\cos\phi_e$ weighting and ω in the ordinate. The corresponding GLM pseudomomentum density $-P\cos\phi_m$ shown in figure 6e in the same coordinate has a very different structure and magnitude. It forms two pairs of negative and positive zones north and south of the forcing region. The pair appearing north of the forcing region is particularly strong, with the maximum value reaching near 50 ms^{-1}, an order of magnitude greater than the maximum $A^*\cos\phi_e$ (note that the contour interval in figure 6e is 30 times greater than that

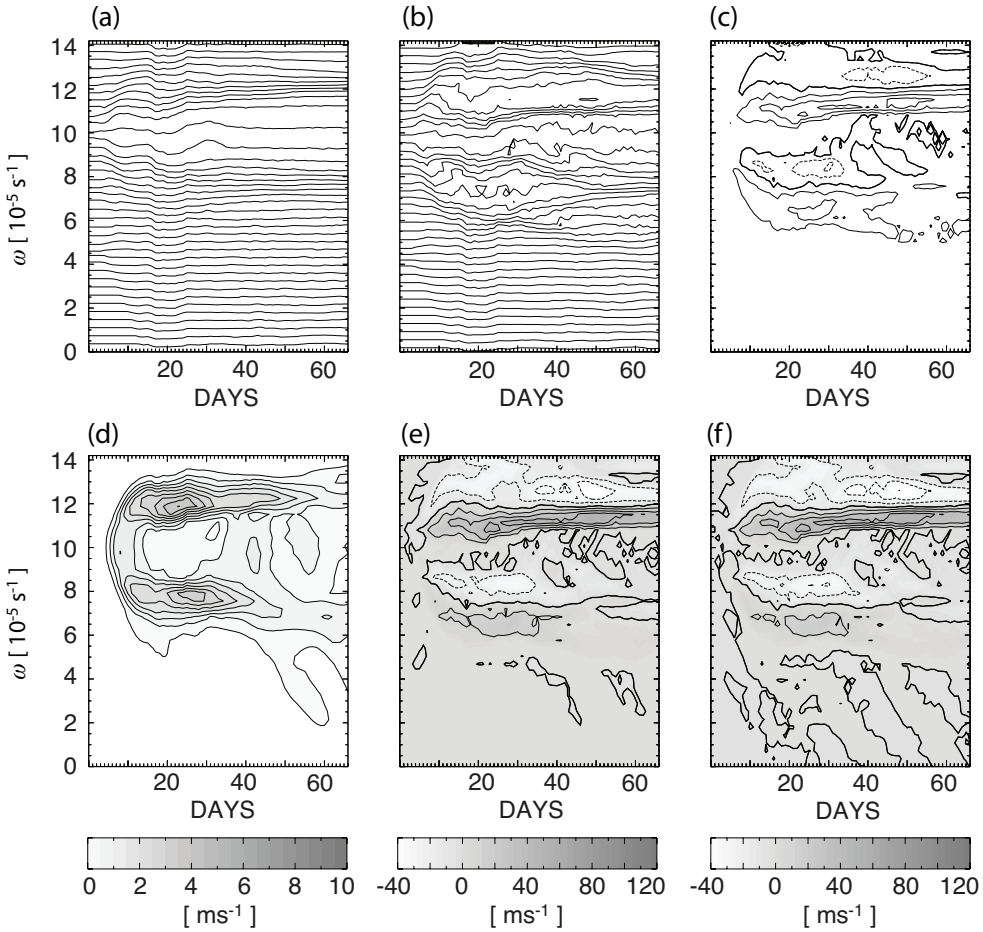

FIGURE 6. (a) Equivalent latitude μ_e for the Northern Hemisphere as a function of time and absolute vorticity. Contour interval is 0.025. (b) Same as (a) but for center-of-mass latitude μ_m. (c) Same as (b) but for $\mu_m - \mu_e$. Negative values are plotted in dashed contours. (d) Same as (a) but for $A^* \cos\phi_e$. Contour interval is 0.5 ms^{-1}. (e) Same as (d) but for the negative of GLM pseudomomentum $-P\cos\phi_m$. Contour interval is 15 ms^{-1} and negative values are dashed. (f) Same as (d) but for $-P\cos\phi_m - A^*\cos\phi_e$. Contour interval is 15 ms^{-1}.

in figure 6d). Even in the early stage of simulation, $-P\cos\phi_m$ is qualitatively different from $A^*\cos\phi_e$, for example it is predominantly negative in high latitudes. Figure 6f shows $-P\cos\phi_m - A^*\cos\phi_e$. According to (2.18), this quantity equals $\overline{M}(\mu_e) - \overline{M}^L$. There is little qualitative difference between figures 6e and f, thus $-P\cos\phi_m$ is dominated by this 'Stokes correction term' and has little bearing on $A^*\cos\phi_e$. From the second identity of (2.38), one sees that this term consists of the impulse associated with the Stokes displacement $\overline{M}(\mu_e) - \overline{M}(\mu_m)$ and the Stokes correction M^S about $\mu = \mu_m$. Given that $\overline{M}(\mu_e) - \overline{M}(\mu_m) \approx a\overline{\omega}(\mu_m - \mu_e)$ when the displacement $\mu_m - \mu_e$ is small, and that the structure of $\mu_m - \mu_e$ in figure 6c qualitatively matches that of $-P\cos\phi_m - A^*\cos\phi_e$ in figure 6f suggest that the impulse of displacement dominates the Stokes correction.

4.3. *Sensitivity to spectral truncation*

To test the sensitivity of the dynamics and diagnostics to the number of retained harmonics, we have repeated the simulation with T63 and T42 truncations. The analyses

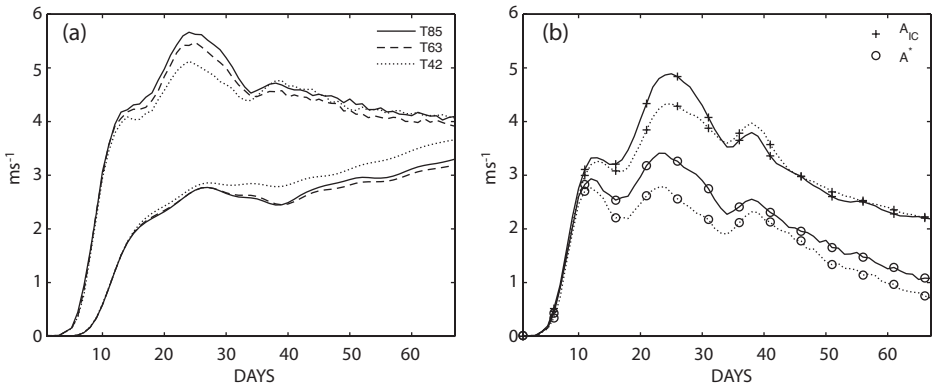

FIGURE 7. (a) Average u_{ref} (curves with larger values) and $\overline{u}$ within the forcing region from three integrations at different truncation; T85 (solid), T63 (dashed) and T42 (dotted). (b) Wave activities in the same region for T85 (solid) and T42 (dotted); $\overline{A_{IC}}$ (+) and A^* (∘).

for these runs are performed using the same 256×128 Gaussian grid. The model parameters are identical except for the hyperdiffusion coefficient, which is adjusted to keep the damping rate for the harmonic with maximum resolved wavenumber unchanged.

Figure 7a shows that u_{ref} in the forcing region is relatively insensitive to the truncation (indicated by the three curves near the top with different line types). There is about 10 percent decrease in the peak value from T85 to T42; this is probably due to the enhanced hyperdiffusion in lower truncation runs since u_{ref} responds to only the nonconservative forcing and dissipation. The zonal-mean flow, which plots lower in figure 7a, is nearly identical for T85 and T63 but shows some *increase* in T42. This suggests that the eddy vorticity flux increases at low resolution, which in turn suggests that the small-scale contributions to the vorticity flux filtered from T42 is negative and not fully compensated by the enhanced hyperdiffusion. This last point is consistent with the notion that vorticity flux at small scales is diffusion-like (down-gradient).

The wave activities in the same region first grow due to forcing and then equilibrate through the E-P flux divergence (figure 7b). Peak values of both A^* and $\overline{A_{IC}}$ decrease appreciably from T85 to T42, but only changes in the former persist for the duration of the simulation.

5. Summary

In recent papers Nakamura and collaborators have introduced a theory for finite-amplitude eddy-mean flow interaction based on a new wave activity, A^*, calculated in terms of the meridional displacement of the contours of PV (or absolute vorticity in the case of barotropic flow) relative to the zonal circle of equivalent latitude. In this article we have investigated the connection between the new theory and the extant formalisms, both theoretically and numerically. The main results are the following.

(1) Both the GLM pseudomomentum density P (Andrews & McIntyre 1978*a*) and the zonal-mean impulse-Casimir wave activity $\overline{A_{IC}}$ (Killworth & McIntyre 1985; McIntyre & Shepherd 1987; Haynes 1988) may be cast into a flux conservation form in equivalent latitude, which may then be related to an exact Eliassen-Palm theorem through gauge transformation ((2.22) and (3.5)). In this sense they are both related to A^*, although only A^* satisfies an exact nonacceleration theorem for the zonal-mean flow $\bar{u}$. However,

under conservative dynamics the global mean values of all three wave activities remain steady.

(2) Both the new and GLM formalisms derive the respective nonacceleration theorem from Kelvin's circulation theorem, but they differ in the way the circulation is partitioned into a mean flow and wave activity/pseudomomentum densities. $A^* \cos\phi_e$ and $-P\cos\phi_m$ differ by the Stokes correction of M relative to the zonal mean at equivalent latitude $\overline{M}(\mu_e) - \overline{M}^L$. The difference does not vanish even at small amplitude and tends to dominate $-P\cos\phi_m$ at finite amplitude, making it very different from $A^*\cos\phi_e$ (e.g., P is not sign-definite). A^* is sign-definite and comparable in magnitude to the angular momentum of the mean flow. The new partitioning of Kelvin's circulation, $C = 2\pi a\cos\phi_e(\overline{u} + A^* + \Omega a\cos\phi_e)$, is more useful for the interpretation of wave-mean flow interactions from gridded data than the one offered by the GLM theory.

(3) A^* converges to the impulse-Casimir wave activity $\overline{A_{IC}}$ and the linear wave activity A_L in the small-amplitude conservative limit, provided that the reference states are identical. At finite amplitude, although the global-mean $\overline{A_{IC}}$ and A^* behave similarly, their local profiles differ substantially. Since A^* satisfies an exact nonacceleration theorem for the zonal-mean flow in the conservative (but finite-amplitude) limit, it has a more direct bearing on the local modification of the zonal-mean flow than $\overline{A_{IC}}$. However, unlike A_{IC} , A^* cannot be defined as a 2D (longitude-latitude) wave activity density, which limits its application to the interaction between the zonal-mean flow and finite-amplitude eddies.

(4) In the spirit of previous PV-equivalent latitude diagnostics (Butchart & Remsberg 1986; Baldwin & Dunkerton 1998), an eddy-free reference state $u_{ref} = \overline{u} + A^*$ is unaffected by the advective flux of eddy vorticity and thus useful for the assessment of nonconservative effects on the flow.

In summary, the theory for finite-amplitude eddy-mean flow interaction based on A^* is a practical alternative to the GLM formalism, which has long been considered unsuitable for data analysis (Shepherd 1983; McIntyre 1980; Andrews *et al.* 1987). The application of the new theory has already proven fruitful, allowing one to quantify from meteorological data alone the quasi-adiabatic adjustment to the mean flow by the eddies (NS10, NS11). The barotropic formulation based on Kelvin's circulation extends naturally to the diagnosis of atmospheric flows in the isentropic coordinate (NS11) but it can be easily adapted to baroclinic quasigeostrohic flows in the isobaric coordinate as well (NS10). Furthermore, A^* can incorporate the effects of mixing through effective diffusivity (Nakamura 1996) of PV, thus providing a separate measure of *irreversible*, non-adiabatic adjustment to the mean flow (NZ10ab).

This research is supported by NSF Grant ATM0750916. Views expressed herein are those of the authors and do not necessarily reflect those of the NSF.

REFERENCES

Allen, D. R. & Nakamura, N. 2003 Tracer equivalent latitude: a diagnostic tool for isentropic transport studies. *J. Atmos. Sci.* **60** (2), 287–304.

Andrews, D. G., Holton, J. R. & Leovy, C. B. 1987 *Middle Atmosphere Dynamics*. Academic Press, 489pp.

Andrews, D. G. & McIntyre, M. E. 1976 Planetary waves in horizontal and vertical Shear: the generalized Eliassen-Palm relation and the mean zonal acceleration. *J. Atmos. Sci.* **33** (11), 2031–2048.

Andrews, D. G. & McIntyre, M. E. 1978*a* An exact theory of nonlinear waves on a Lagrangian-mean flow. *J. Fluid Mech.* **89** (04), 609–646.

Andrews, D. G. & McIntyre, M. E. 1978*b* Generalized Eliassen-Palm and Charney-Drazin theorems for waves in axismmetric mean flows in compressible atmospheres. *J. Atmos. Sci.* **35** (2), 175–185.

Andrews, D. G. & McIntyre, M. E. 1978*c* On wave-action and its relatives. *J. Fluid Mech.* **89** (04), 647–664.

Baldwin, M. P. & Dunkerton, T. J. 1998 Biennial, quasi-biennial, and decadal oscillations of potential vorticity in the northern stratosphere. *J. Geophys. Res.* **103(D4)**, 3919–3928.

Boer, G. J. & Shepherd, T. G. 1983 Large-scale two-dimensional turbulence in the atmosphere. *J. Atmos. Sci.* **40** (1), 164–184.

Brunet, G. & Haynes, P. H. 1996 Low-latitude reflection of Rossby wave trains. *J. Atmos. Sci.* **53** (3), 482–496.

Bühler, O. 2009 *Wave and Mean Flows*. Cambridge University Press, 370pp.

Butchart, N. & Remsberg, E. E. 1986 The area of the stratospheric polar vortex as a diagnostic for tracer transport on an isentropic surface. *J. Atmos. Sci.* **43** (13), 1319–1339.

Charney, J. G. 1959 Hydrodynamics of the atmosphere and numerical weather prediction-a synthesis. *Proc. Nat. Acad. Sci.* **45** (12), 1650–1655.

Charney, J. G. & Drazin, P. G. 1961 Propagation of planetary-scale disturbances from the lower into the upper atmosphere. *J. Geophys. Res.* **66**, 83–109.

Edmon, H. J., Hoskins, B. J. & McIntyre, M. E. 1980 Eliassen-Palm cross sections for the troposphere. *J. Atmos. Sci.* **37** (12), 2600–2616.

Eliassen, A. & Palm, E. 1961 On the transfer of energy in stationary mountain waves. *Geofys. Publ.* **22(3)**, 1–23.

Harvey, V. L., Randall, C. E. & Hitchman, M. H. 2009 Breakdown of potential vorticity-based equivalent latitude as a vortex-centered coordinate in the polar winter mesosphere. *J. Geophys. Res.* **114** (D22105).

Haynes, P. H. 1988 Forced, dissipative generalizations of finite-amplitude wave-activity conservation relations for zonal and nonzonal basic flows. *J. Atmos. Sci.* **45** (16), 2352–2362.

Held, I. M. 1985 Pseudomomentum and the orthogonality of modes in shear flows. *J. Atmos. Sci.* **42**, 2280–2288.

Held, I. M. & Phillips, P. J. 1987 Linear and nonliear barotropic decay on the sphere. *J. Atmos. Sci.* **44** (1), 200–207.

Killworth, P. D. & McIntyre, M. E. 1985 Do Rossby-wave critical layers absorb, reflect, or over-reflect? *J. Fluid Mech.* **161** (1), 449–492.

Kuo, H.-L. 1951 Vorticity transfer as related to the development of the general circulation. *J. Meteor.* **8** (5), 307–315.

Liberato, M. L. R., Castanheira, J. M., de la Torre, L., DaCamara, C. C. & Gimeno, L. 2007 Wave energy associated with the variability of the stratospheric polar vortex. *J. Atmos. Sci.* **64** (7), 2683–2694.

Magnusdottir, G. & Haynes, P. H. 1996 Wave activity diagnostics applied to baroclinic wave life cycles. *J. Atmos. Sci.* **53** (16), 2317–2353.

Magnusdottir, G. & Haynes, P. H. 1999 Reflection of planetary waves in three-dimensional tropospheric flows. *J. Atmos. Sci.* **56** (4), 652–670.

McEwan, A. D., Thompson, R. O. R. Y. & Plumb, R. A. 1980 Mean flows driven by weak eddies in rotating systems. *J. Fluid Mech.* **99** (03), 655–672.

McIntyre, M. E. 1980 Towards a Lagrangian-mean description of stratospheric circulations and chemical transports. *Phil. Trans. Roy. Soc. London. Ser. A, Math. Phys. Sci.* **296** (1418), 129–148.

McIntyre, M. E. 1982 How well do we understand the dynamics of stratospheric warmings? *J. Meteor. Soc. Japan.* **60**, 37–65.

McIntyre, M. E. & Shepherd, T. G. 1987 An exact local conservation theorem for finite-amplitude disturbances to non-parallel shear flows, with remarks on Hamiltonian structure and on Arnol'd's stability theorems. *J. Fluid Mech.* **181** (1), 527–565.

Nakamura, N. 1995 Modified Lagrangian-mean diagnostics of the stratospheric polar vortices. Part I. Formulation and analysis of GFDL SKYHI GCM. *J. Atmos. Sci.* **52** (11), 2096–2108.

Nakamura, N. 1996 Two-dimensional mixing, edge formation, and permeability diagnosed in an area coordinate. *J. Atmos. Sci.* **53** (11), 1524–1537.

Nakamura, N. & Solomon, A. L. 2010 Finite-amplitude wave activity and mean flow adjust-

ments in the atmospheric general circulation Part I. Quasigeostrophic theory and analysis. *J. Atmos. Sci.* **67** (12), 3967–3983.

Nakamura, N. & Solomon, A. L. 2011 Finite-amplitude wave activity and mean flow adjustments in the atmospheric general circulation Part II: Analysis in the isentropic coordinate. *J. Atmos. Sci.* **68**, accepted.

Nakamura, N. & Zhu, D. 2010*a* Finite-amplitude wave activity and diffusive flux of potential vorticity in eddy-mean flow interaction. *J. Atmos. Sci.* **67** (9), 2701–2716.

Nakamura, N. & Zhu, D. 2010*b* Formation of jets through mixing and forcing of potential vorticity: analysis and parameterization of beta-plane turbulence. *J. Atmos. Sci.* **67** (9), 2717–2733.

Reynolds, O. 1895 On the dynamical theory of incompressible viscous fluids and the determination of the criterion. *Phil. Trans. Roy. Soc. London. A* **186**, 123–164.

Scinocca, J. F. & Peltier, W. R. 1994 The instability of Long's stationary solution and the evolution toward severe downslope windstorm flow. Part II: The application of finite-amplitude local wave-activity flow diagnostics. *J. Atmos. Sci.* **51** (4), 623–653.

Shepherd, T. G. 1983 Mean motions induced by baroclinic instability in a jet. *Geophys. Astrophys. Fluid Dyn.* **27**, 35–72.

Shepherd, T. G. 1988 Rigorous bounds on the nonlinear saturation of instabilities to parallel shear flows. *J. Fluid Mech.* **196** (1), 291–322.

Shepherd, T. G. 1989 Nonlinear saturation of baroclinic instability. Part II: Continuously stratified fluid. *J. Atmos. Sci.* **46** (7), 888–907.

Strong, C. & Magnusdottir, G. 2008 How rossby wave breaking over the pacific forces the north atlantic oscillation. *Geophys. Res. Lett.* **35** (L10706).

Vallis, G. K. 2006 *Atmospheric and Oceanic Fluid Dynamics*. Cambridge University Press, 745pp.